

## Electric field measurements in high pressure discharges

**S.V. Mitko, V.N.Ochkin, A.Yu.Serdyuchenko, S.N.Tskhai**

Lebedev Physical Institute, Russian Academy of Science  
Leninski prosp., 53, Moscow, Russia

**D.A.Akimov, D.A.Sidorov-Biryukov, D.V. Sinyaev, A.M.Zheltikov**

Lomonosov Moscow State University  
Vorobievsky Gori, Moscow, Russia

### I. Introduction

Electric fields define a wide range of interactions and phenomena at different phases of matter both on micro- and macro-level. Investigation of electric fields behavior provides a key for understanding of these phenomena and their application.

Lets consider a problem of investigation of electric fields measurements in gases and plasma by methods of optics and spectroscopy.

Plasma, as being the partly (or in full – so called “hot” plasma, which isn’t under consideration here) ionized gas has some essential difference in comparison with gas, namely plasma object possesses the property of quasineutrality. The last one is satisfied by the fact that the conception of plasma can be attributed only to a matter with sufficiently large size, defined by so-called Debye radius

$$r_D = \left( \frac{kT_e}{4\pi e^2 n_e} \right)^{1/2}, \quad (1)$$

where  $n_e$ ,  $T_e$  and  $e$  – are density, temperature and charge of electron,  $k$  is Boltzman constant. If one expresses  $T_e$  in K,  $n_e$  in  $\text{cm}^{-3}$ , then  $r_D \approx 5 \sqrt{\frac{T_e}{n_e}}$

In most cases plasma is created and operated by applying the external field. The self-consistent spatial field configurations inside the plasma can be highly complicated by interactions with space charges, and they are an important subject for investigations, when the individual discharge media elements haven’t to be plasma in common sense.

It has to be noted that in case of plasma created not by external field and by, for example, heating (thermal plasma), then the internal electric fields play an important role as well, since space charge isn’t compensated in every elementary volume  $n_e \neq n_i$  and local statistic field is generated. The magnitude of local fields can achieve high value

$$E_0 = 2\pi \left( \frac{4}{15} \right)^{2/3} e n_e^{2/3} \approx 1.27 \cdot 10^{-6} n_e^{2/3}. \quad (2)$$

Conventional approaches to the problem of electric field measurements with the laser help include various modifications of the Stark effect and laser induced fluorescence of Rydberg states [1, 2, 3]. These methods permit a very good spatial resolution and a high sensitivity of electric-field measurements to be achieved. However, these techniques usually work well and efficient only for low gas pressures (typically less than 1 Torr), since collisions begin to play an important role, perturbing atomic states, and background plasma emission considerably reduces the sensitivity of such measurements at higher gas pressures.

So, the plasma neutral and charged particles density is a serious factor limiting not only classical but also laser methods when using the optical electronic transitions. It is the fundamental problem to overcome this limitation.

One of the important factors in the mechanism of these limitations is that despite the fact of using the lasers the cycle absorption-emission is not coherent in time. From this point of view the special interest represents the recently invented coherent 4-wave mixing scheme in the presence of E-field [4, 5], namely coherent anti-stokes Raman scattering (CARS).

## II. Four-wave mixing technique for E-field measurements.

The scheme proposed looks as a known CARS scheme. The versions are compared in fig.1. Case 1a – non-degenerate CARS, 1b – degenerate CARS. The new proposal is the 1c scheme; let's call it as CRS. If one compare 1a and 1c it follows that the last one is the specific case with  $\omega_3 = 0$ . In this particular case the static field acts as a field with zero frequency. Then the quantitative description follows the usual CARS formalism. In the new scheme the generated IR radiation has the intensity:

$$I_{ir} \sim \left| \chi_{ir}^{(3)} \right|^2 I_1 I_2 E^2 I^2, \quad (3)$$

where  $I_1, I_2$  – intensities of waves  $\omega_1, \omega_2, l$  – effective interaction length,  $\chi^{(3)}$  – tensor of nonlinear susceptibility. Intensity of degenerated CARS-signal is

$$I_{CARS} \sim \left| \chi_{CARS}^{(3)} \right|^2 I_1^2 I_2 I^2. \quad (4)$$

Both susceptibilities are proportional to the population difference, so that the ratio of signals  $I_{CARS}/I_{ir}$  depends only on  $E^2$  (if the intensity  $I_1$  is kept fixed). The absolute calibration for E can be obtained by measuring the IR and CARS intensities. The E-field can evidently also be of AC nature. In this case the IR-signal will simply be generated at the side-band frequency and the intensity will be proportional to the square of the field peak value.

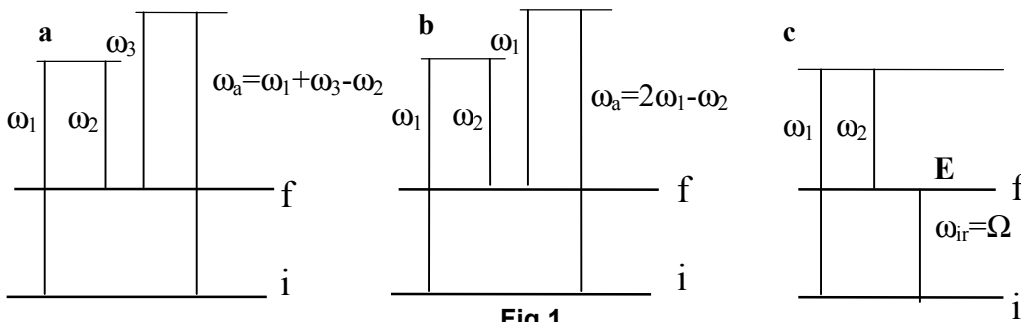


Fig.1  
Optical transitions in case of a) non-degenerated CARS, b) degenerated CARS, c) IR radiation generation in a presence of dc field - CRS.

The experiment was performed in hydrogen in the presence of a static field. For measurements a CRS process  $\omega_{CRS} = \omega_3 + \omega_1 - \omega_2$  was employed, where the frequency difference

$\omega_1 - \omega_2$  was tuned to a Raman-type resonance with a frequency  $\Omega$  of the  $Q(1)$  transition ( $\nu = 0, J = 1 \rightarrow \nu = 1, J = 1$ ) of a hydrogen molecule in the  $X^1\Sigma_g^+$  ground electronic state ( $\lambda = 2.4 \mu\text{m}$ ).

The experiment setup, based on the modified CARS spectrometer, is shown in fig.2. The experimental system consists of a master oscillator, crystals for frequency doubling, a dye laser, a chamber, filled with hydrogen, and a detection system. As a master oscillator, Nd:YAG laser was employed, producing radiation with a wavelength of  $1.06 \mu\text{m}$ , pulse repetition rate of 20 Hz, and

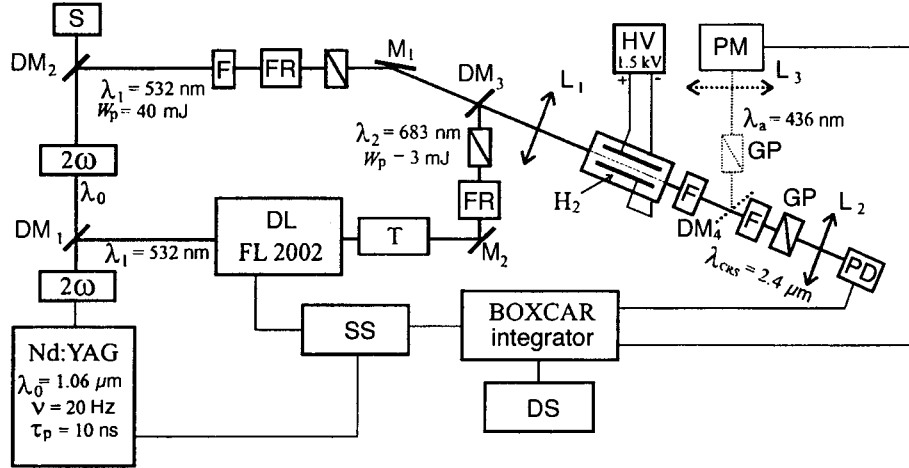


Fig.2

**Experimental setup,  $2\omega$  - frequency-doubling crystals; DL-dye laser; SS – synchronization system; DS – detection system; PM – photomultiplier; PD –IR detector; T – telescope;  $M_1, M_2$  – mirrors,  $DM_1 \dots DM_4$  – dichroic mirrors, GP – Glan prism, F – filters, FR – Fresnel rhombs; S – screen; HV – high –voltage source,  $L_1$ -  $L_2$  – lenses**

pulse duration of 10 ns. A DKDP crystal was used to convert fundamental radiation of this Nd:YAG laser into the second harmonic. Thus, a pump wave with the frequency  $\omega_1$  (corresponding to the wavelength of 532 nm) and pulse energy of 40 mJ was produced. The second harmonic was also used to pump the dye laser, which generated the radiation at a wavelength of 683 nm (frequency  $\omega_2$ ), pulse energy of 3 mJ, and a bandwidth of  $0.2 \text{ cm}^{-1}$ . The light beams of the second harmonic and dye-laser radiation were brought in coincidence in space with the use of dichroic mirrors and were focused into a chamber filled with hydrogen.

The modification consists of an additional optical channel to detect the IR radiation. The CRS signal generated in a chamber was detected with an InSb IR detector and was processed with a BOXCAR integrator. A two-channel BOXCAR integrator processes both the CARS and IR signals so that their ratio can be plotted.

Fig.3 gives the experimental dependence of the IR signal intensity on the electric field strength. The experiment was performed in hydrogen, at the pressure 1 atm. As predicted, the

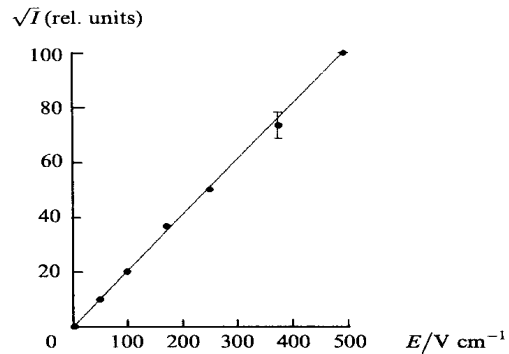
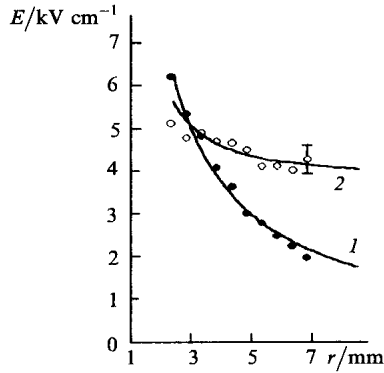


Fig.3

**Experimental dependence of the infrared radiation intensity on the intensity of a static electric field**

square root of intensity is proportional to field strength. Under described above conditions the minimum field observable by our IR detection scheme was 50 V/cm. With the help of up-conversion scheme the sensitivity of 20 V/cm was demonstrated. The practical limit was given by electric interference from the YAG pump laser power supply.

Because of the coherency of all fields the influence of gas pressure is strongly damped.



**Fig. 4**

**Radial distribution of the electric field intensity (1) electrostatic solution for  $I=0$ ; (2) corona discharge in  $H_2$  for  $I=270 \mu A$**

The limiting factor, at pressure higher than 10 atm is the phase mismatching because of media dispersion.

Fig. 4 shows an example of electric field measurements in a corona discharge in hydrogen. The corona electrode is a thin wire stretched along the axis of a cylinder of radius  $r_1=8.5\text{mm}$ . A voltage of  $U=7\text{ kV}$  was maintained between the electrodes. The onset of the corona discharge is governed by the hydrogen pressure in the cell and was monitored by recording the current through the discharge gap. At a hydrogen pressure of 10 bar there was no current flowing. In this case the electric field distribution corresponds to the solution of Poisson's

equation. This solution is represented by curve 1. The dots are our measured points. At 1.6 bar pressure the measured current was 270 mA. Due to the formation of space charges determined by the mobility of ions, the field distribution is distorted. It is also possible to calculate the pertinent field distribution (curve 2). The open circles are again our measured points. Good agreement is established.

### III. Microfields influence

Let us briefly discuss one more aspect concerning this method, which is rather specifically related to field measurements in plasmas. All electric field dependent spectral measurements have the problem to distinguish between the influence of macroscopic and microscopic fields. The last ones are due to local non-neutrality on the scale of the Debye length.

For all non-coherent Stark-based optical methods (including also the linear and nonlinear laser excitation of fluorescence) the resulting effect is simply the sum of actions of the regular field and statistical microfields. The situation is completely different in the last case considered here. It is easy to see when using a slightly extended form of above equation for CARS intensity, which indicates that the intensity of the electric field stimulated CARS signal grows with the square of the effective length  $l$  (4).

The signal is generated in the focus region of the laser beams, which, for the collinear case, is approximately given by the cylinder

$$D = \frac{4 \lambda f}{\pi d}; l = \frac{3 \pi D^2}{\lambda} \quad (5)$$

The IR signal stimulated by the regular electric field to be measured is given by (3). The resulting sum of the incoherent intensity stimulated by the microscopic field will be

$$I_{ir}^{(\mu)} \sim |\chi_{ir}^{(3)}|^2 I_1 I_2 E_\mu^2 l r_D, \quad (6)$$

because  $r_D$  is the estimate for microfield correlation length, which can be taken approximately as a Debye length (1) (in more details this problem was studied recently in [6]).

The ratio of these components is therefore:

$$\gamma = \frac{I^{(\mu)}}{I} \sim \frac{E_\mu^2 r_D}{E^2 l}. \quad (7)$$

Let us consider the case of  $l = 1$  mm and  $T = 2$  eV. Curve 1 in fig.5 demonstrates values of the regular electric field that can be measured. For this estimate it was assumed that the regular

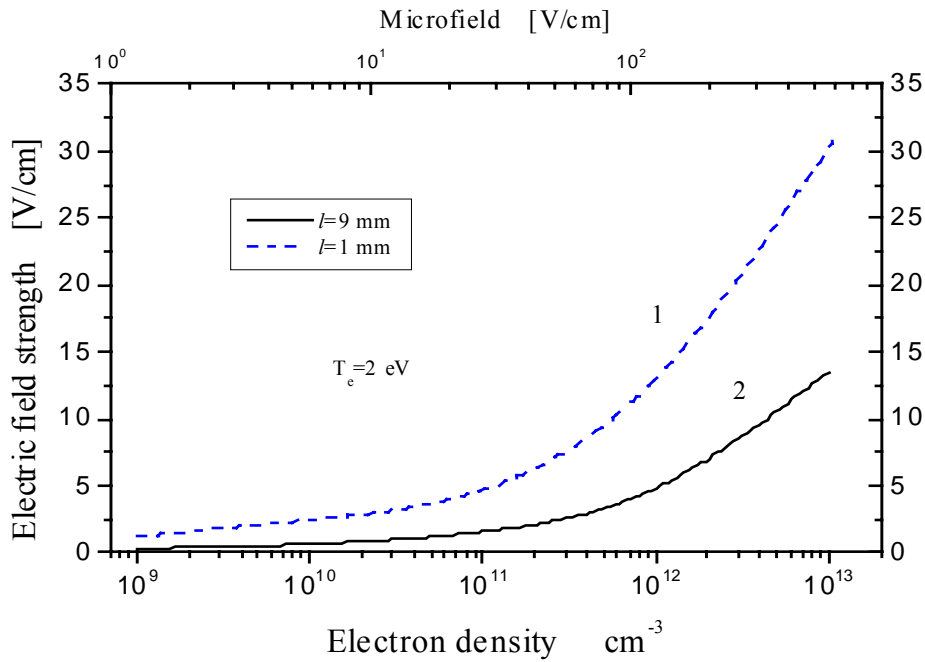


**Fig.5**

**The curves of equality of IR intensities induced by electric field correlated over the focusing region with those by microfields for different electron densities and focusing parameters .  
T<sub>e</sub>=2eV**

field and microwave fields give the same contribution to the full signal

$$I^S = I_{ir} + I_{ir} \mu.$$

It becomes clear that the values of microfield strength are much higher in this case than the measurable regular field, but the regular field can be measured. The situation is even more pronounced for  $l = 9$  mm (curve 2). It has to be mentioned that the first results are of the sense of estimate. The quantitative problem is more complicated and the more precise form of plasma microfields correlations has to be taken into account. This problem is not solved finally but it is important and can elucidate the possibilities of electron component studies at plasma densities much higher than it is possible by other methods.

#### IV. Polarization-sensitive measurements of the electric field by means of CRS

The special question is the vector sensitivity of CRS scheme. The main idea of using a dc-field-induced CRS for determination of the electric field direction is based on the fact that, if a dc or quasi-static electric field is involved as a zero-frequency wave in nonlinear-optical Raman-resonant process, the amplitude, the phase, and the polarization of the resulting coherent signal depend on the properties of this dc or quasi-static electric field. Thus, polarization measurements on the signal produced through a coherent Raman process can be generally performed to determine the orientation of the dc or quasi-static electric field.

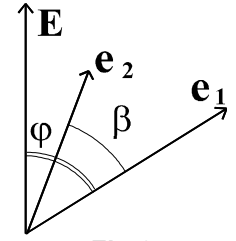


Fig.6  
Vectors orientations

Following the above mentioned analogy it's possible to use the known CARS theory to write the peak and polarization expressions for scattering. For isotropic cubic-nonlinear media and three pumping waves the vector of non-linear polarization can be defined by means the components of third-order susceptibility tensor  $\chi_{ijkl}^{(3)} = \chi_{ijkl}^{(3)}(\omega_{CRS}; \mathbf{0}, \omega_1, -\omega_2)$  and the electric vectors of pumping waves. When omitting the frequency arguments

$$\vec{P}^{(3)} = D \left\{ \chi_{1122}^{(3)} \vec{E} (\vec{E}_1 \vec{E}_2^*) + \chi_{1212}^{(3)} \vec{E}_1 (\vec{E} \vec{E}_2^*) + \chi_{1221}^{(3)} \vec{E}_2 (\vec{E} \vec{E}_1^*) \right\}, \quad (8)$$

Here  $D$  – coefficient,  $\vec{E}_1, \vec{E}_2$  are the electric vectors of pumping waves with frequencies  $\omega_1$  and  $\omega_2$  correspondingly;  $\vec{E}$  – vector of dc electric field.

When the polarizations  $\mathbf{e}_1, \mathbf{e}_2$  of pumping laser beams are in parallel ( $\beta=0$ , see fig.6) and have an angle  $\varphi$  with the direction of dc electric field, then

$$\vec{P}^{CRS} = \left\{ \chi_{1122}^{(3)} \vec{e} + \chi_{1212}^{(3)} \cos(\varphi) \vec{e}_1 + \chi_{1221}^{(3)} \cos(\varphi) \vec{e}_2 \right\} E_1 E_2 E, \quad (9)$$

$$\alpha(\varphi) = \arcsin \left( \frac{1}{2} \frac{\eta \sin(2\varphi)}{\sqrt{1 + \eta(\eta + 2) \cos^2(\varphi)}} \right), \quad \eta = \frac{\chi_{1212}^{(3)} + \chi_{1221}^{(3)}}{\chi_{1122}^{(3)}}, \quad (10)$$

where  $\vec{e}$  – unit vector of the polarization of the dc electric field;  $E_1, E_2$  and  $E$  – are amplitudes of the pumping waves with frequencies  $\omega_1, \omega_2$  and dc field correspondently;  $\alpha(\varphi)$  – is an angle between the polarization vector  $\mathbf{e}_{CRS}$  of the CRS signal and the direction of the dc electric field  $\mathbf{E}$ . From (8) one can get the amplitude of electric field intensity and also the angles between vectors of polarization of the waves. So the direction of electric field is easy to get from measuring of CRS polarization in an experiment. In [7] the polarization properties of CRS signal in molecular hydrogen have been investigated. In the preliminary calibrating experiments

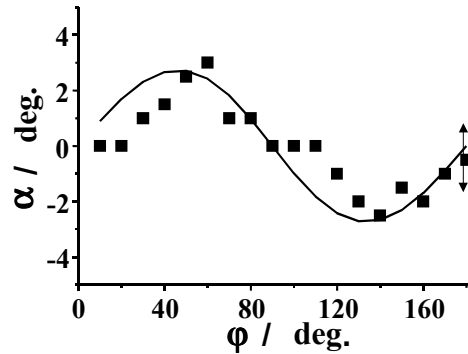


Fig.7

Dependence of the angle  $\alpha$  between the polarization vector of the CRS signal and the direction of a dc electric field  $\mathbf{E}$  on the angle  $\varphi$  between the dc field and a pair of collinear polarization vectors  $\mathbf{e}_1$  and  $\mathbf{e}_2$  of biharmonic pump waves.

an electric field (up to 5 kV) was applied to the parallel plane plates, placed in the chamber, filled with molecular hydrogen at the pressure of  $\sim 1$  atmosphere. In fig.7 the angle  $\alpha$  between the polarization vector  $\mathbf{e}_{\text{CRS}}$  of the CRS signal and the direction of the dc electric field  $\mathbf{E}$  is shown as a function of angle  $\varphi$  between the direction of the dc field and the collinear pump vectors  $\mathbf{e}_1$  and  $\mathbf{e}_2$ . In general the electric field vector can be determined from maximum CRS signal over rotating of the collinear vectors  $\mathbf{e}_1$  and  $\mathbf{e}_2$ . However, the difference between maximum and minimum of the signal in such experiment strongly depend on Raman scattering tensor properties, and for symmetrical hydrogen molecules this difference is very small (see fig.7), so the precision of such kind of measurements is limited. Other hand namely this circumstance allows the simple direct measurements. The collinear vectors of pumping laser  $\mathbf{e}_1$  and  $\mathbf{e}_2$  were fixed. By using the polarization analyzer placed before detector the polarization of CRS signal was measured and the angle between polarization of the signal and pumping laser beams was determined. The deviation of electric field vector from polarization of CRS signal can be measured or can be calculated, (if the invariants of Raman scattering tensor are known) as one can see in fig.7. These corrections for  $\text{H}_2$  molecules will be small, but can be taken into account.

### V. Time-resolved polarization-sensitive measurements of the electric field in a sliding discharge

As an example of application of polarization-sensitive CRS technique will consider the case of high-power atmospheric-pressure sliding discharge over the surface of material with finite conductivity.

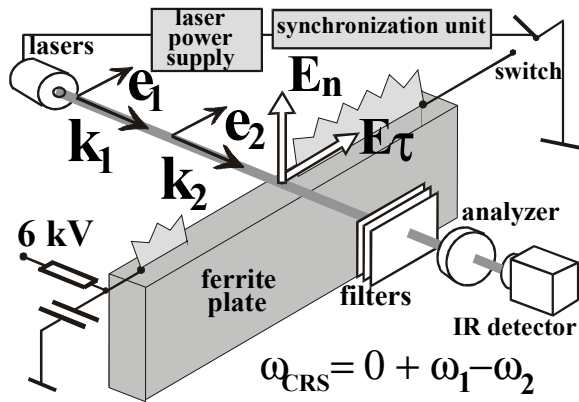


**Fig.8**  
Scheme of the discharge, sliding on the surface of the ferrite

As an example of application of polarization-sensitive CRS technique will consider the case of high-power atmospheric-pressure sliding discharge over the surface of material with finite conductivity. This type of discharge is of practical interest as a high-brightness light source. The physical problem is to determine the mechanism of propagation of the streamer of arc channel. The situation is strongly dependent on the dynamics of electric field in the vicinity of streamer, which is not stationary in time, space and direction.

Experimental setup is shown in fig.2. The scheme of ferrite installation, placed inside the chamber is shown in Fig.8. A  $1 \times 0.1 \text{ cm}^2$  cross-section and 2 cm long NiMn ferrite plate with conductivity of  $0.5 \text{ Ohm}^{-1} \text{ cm}^{-1}$  (at typical voltages applied) has been used to guide the discharge. To avoid the bending of arc channel, the glass plates were pressed to

the wide sides of the ferrite plate. Metal electrodes, pressed to the narrow side of the ferrite at distances from 4 to 12 mm apart each other, formed discharge gap. Discharge was powered by capacitor, charged up to 6 kV. Experiments were carried out in chamber filled with molecular hydrogen at atmospheric pressure. The discharge repetition rate was 5 Hz. The triggering of the discharge was synchronized with the probe laser pulse and could be changed thus it was possible to make measurements during the discharge development.

The laser beams have been directed normally to the discharge channel and focused close to ferrite surface. The waist of focused beams was about 0.1 mm. The polarization of both laser beams was in parallel with direction of discharge channel.

The scattered light and the emission of the discharge were registered by the photodiode making use the control of the delay time between the discharge triggering and the start of the probe laser. Typical signal of the photodiode is shown in Fig.9. The measurements were made at the time of the narrow peak in Fig.9 related to the scattered laser light. The probe laser triggering was delayed relatively the discharge triggering at time interval under control.

Before the discharge is switched on, the electrodes and the ferrite plate are under equal electric potential. It means that at this moment the vector of electric field intensity has the only

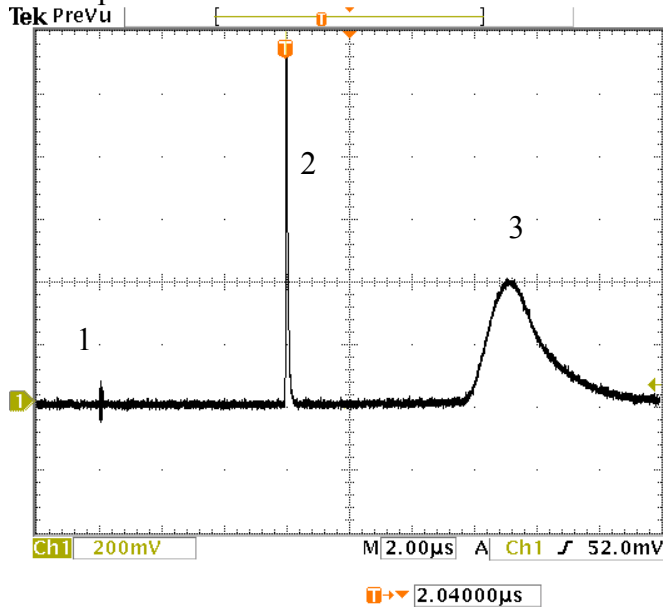


**Fig.9**  
**Typical triggering signals. 1 – triggering moment; 2 – laser pulse; 3 – discharge fluorescence**

component normal to the ferrite surface.

Polarization measurements showed that the CRS polarization and, correspondingly, the vector of electric field intensity are really normal to the ferrite surface.

At the moment of the discharge triggering the connection of the cathode to the ground leads to the redistribution of the electric field pattern. The electric potential decreases linearly from the high positive value at the anode to the zero at the cathode and the tangential electric field component directed to the cathode appears in this case. The angle of the

electric vector depends on the ratio between the tangential and normal components.

Anode and cathode-directed plasma channels start to extend under the action of the tangential electric field. The speed of the anode-directed plasma channel exceeds more than ten times the speed of the cathode-directed channel. The tip of the anode-directed plasma channel has in fact the zero (ground) potential due to the high plasma conductivity. As the plasma front is getting closer to the point of observation the ratio of the electric field components is changing and it is possible to observe the spatial rotation of the electric field vector. Also the increasing of the electric field intensity is observed in this situation (fig.10). The interelectrode voltage is shown in fig.10a. Using the polarization analyzer before the IR detector we could measure the time behavior of the normal (analyzer is normal to the discharge axis) and tangential (analyzer is collinear with discharge axis) electric field components. The results of these measurements are shown in Fig.10b, 10c correspondingly. The electrodes were spaced by 11mm. The data were taken from the space point distanced 3mm from the anode and 1mm up the ferrite surface.

To get the absolute value of the electric field intensity one can use the signal, corresponded to the tangential electric field component at the initial moment of the discharge

development when this component is known (applied voltage divided by the interelectrode distance) By this way it's possible to calibrate the measurements scheme. The intensity of the normal component was found from the ratio of signal intensities for parallel and transversal analyzer positions. It should be noted that the intensity of the normal component is comparable to the tangential one.

Our measurements showed that the tangential component increases slowly and reaches its peak value at the moment the plasma tip passes the point of observation. The maximum of the tangential electric field component is  $\sim 3$  kV/cm.

The behavior of the normal component of the electric field is quite similar. It increases in time and gets the maximum of 3 kV/cm at the same time as the tangential one. Thus in the vicinity of the plasma tip, the vector of the electric field has an angle of 45 degrees to the discharge axis.

Our method makes it possible to measure the small rotation of the electric field vector during the discharge development. The temporal evolution of the angle between the discharge axis and the electric field vector is shown in Fig.10d.

The arc sliding mechanism up to now is not clear definitely. The velocity of sliding keeps approximately the same during propagation. The only fast acceleration can be observed in the final stage of full breakdown. So for a known inter-electrode length and full time of breakdown it is possible to find the streamer velocity. In our conditions this value is  $\sim 1.5 \cdot 10^5$  cm/sec. Other hand the measured value of tangential E-field component gives the close value for electron drift velocity  $\sim 2 \cdot 10^5$  cm/sec. The relatively small E-field peak value  $\sim 3$  kV/cm at the position of the leader front makes the mechanism of direct electron-impact ionization as low effective. For this mechanism

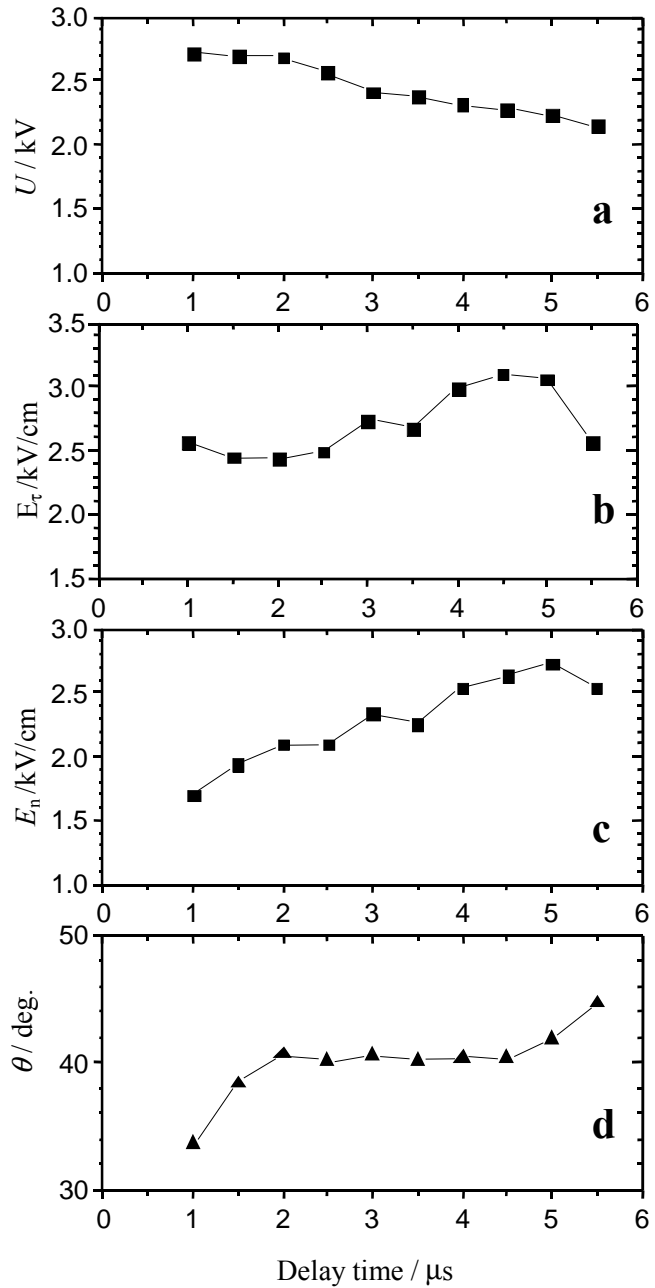


**Fig.10**  
**Time behavior of a) interelectrode voltage, b)- c) tangential and normal component of the electric field, d) angle between the discharge axis and the electric field vector**

the E-field peak value has to be not less  $\sim 12$  kV/cm to provide the first Townsend coefficient  $\sim 1$  cm<sup>-1</sup>. The speed of propagation is too fast to be attributed to the thermal conductivity with consequent heat ionization mechanism. The practical equality of propagation and drift velocity shows that the mechanism of propagation is the existence of high-current (tens of Amps) virtual cathode with thermal ionization just near it in processes of electron-heavy particles multiple collisions.

## VI. Conclusion

The analysis of general polarization properties of a dc-field-induced coherent Raman scattering provides the convenient method for nonintrusive local measurements of micro- and dc-electric fields.

We experimentally studied the properties of the IR signal generated through coherent Raman scattering involving the  $Q(1)$  transition ( $\nu = 0, J = 1 \rightarrow \nu = 1, J = 1$ ) of a hydrogen molecule in the presence of the dc electric field and quasi-static electric field of the sliding discharge propagating along a ferrite surface in a hydrogen atmosphere. At a first time in the practice of studies of pulsed discharges the dynamics of local E-field peak value and vector reorientation was observed experimentally.

The behavior of normal and tangential components gives the possibility to propose the mechanism of arc propagation, which differs from considered earlier.

The results obtained demonstrate the possibilities of CRS-scheme for wide class of objects with dynamic and non-uniform electric fields where other methods of measurements meet the fundamental limitations.

The works are partially supported by the Scientific and Educational Center "Basic Optics and Spectroscopy" (Projects A0133, A0155) of the Program "Integration" and Russian Foundation for Basic Research Grant No.99-02-16339.

- 
1. U.Charnetzki, D.Luggenholsher, H.F.Doebele. Phys.Rev.Letts, v.81, 21, p.4532-4595, (1998)
  2. C.A.Moore e.a. Phys.Rev.Lett., v.52, N7, p.538, (1984).
  3. J.P.Booth, M.Fadallah, J.Derouard, N.Sadeghi. Appl.Phys.Lett., v.65, 7, p.819-821, (1994)
  4. V.P. Gavrilenko, E.B. Kupriyanova, D.P. Okolokulak, V.N. Ochkin, S.Yu. Savinov, S.N.Tskhai, A.N. Yarashev. JETP Lett. (USA), v.56, No 1, p.1-4, (1992).
  5. O.A.Evsin, E.B.Kupryanova, V.N.Ochkin, S.Yu.Savinov, S.N.Tskhai. Quantum Electronics v.25, No3, p.278-282, (1995)
  6. A.M.Zheltikov, N.I.Koroteev, A.N.Naumov, V.N.Ochkin, S.Yu.Savinov, S.N.Tskhai. Quantum Electronics, v.29, No1, p.73-76 (1999)
  7. D.A. Akimov, A.M. Zheltikov, N.I. Koroteev, A.N. Naumov, A.Yu. Serdyuchenko, D.A. Sidorov-Biryukov, A.B. Fedotov, V.N. Ochkin, S.N. Tskhai. JETP Letters v.70, No 6, p.375 (1999).